AGN EVOLUTION REVEALED FROM X-RAY SURVEYS

Yoshihiro Ueda

Department of Astronomy, Kyoto University, 606-8502 Kyoto, Japan

ABSTRACT

I review the cosmological evolution of Active Galactic Nuclei (AGNs) revealed from X-ray surveys, mainly based on studies by using hard (>2 keV) X-ray selected samples. The hard X-ray luminosity function of type-1 and type-2 AGNs is well described by the luminosity dependent density evolution, where the cut-off redshift of density evolution increases with luminosity. This suggest anti-hierarchical (or down-sizing) growth of supermassive black holes in galactic centers. The black hole mass function at $z < 1$ can be explained, on average, as the consequence of "standard" accretion with a radiative efficiency of ≈ 0.1. Population synthesis models constructed from the observational results of hard X-ray luminosity function and absorption function of AGNs are now close to finalization. However, toward complete understanding of the X-ray background origin, there still remains several issues to be solved by current and future missions.

Key words: X-rays; AGN; Surveys; X-ray Background.

1. INTRODUCTION

The X-ray background (XRB) is the integration of emission from all accreting black holes in the universe, and hence carries key information on the growth history of supermassive black holes (SMBHs) in galactic centers. The tight correlation between bulge mass and black-hole mass in the local universe indicates a strong link between formation of stars and that of SMBHs. Thus, revealing the accretion history of SMBHs is a crucial issue, to which X-ray astronomy should give a definitive answer, for understanding the whole history of the universe including galaxy formation processes.

To solve the XRB origin is equivalent to revealing the cosmological evolution of AGNs that constitute the XRB. Since the discovery of the XRB in 1962, efforts to resolve the XRB by surveys with increasing sensitivities have been main stream of extra-galactic X-ray astronomy. Figure 1 shows a summary of log N log S relations in the

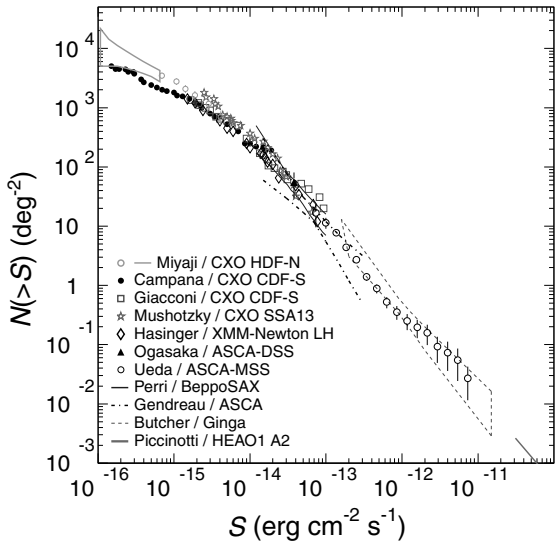

Figure 1. Log N log S relations in the 2–10 keV band obtained from various X-ray surveys. Complied by Kushino et al. (2002).

2–10 keV band determined with various hard X-ray satellites. Thanks to the heritage from past X-ray satellites together with the recent missions, Chandra and XMM-Newton, that have mostly resolved the faintest part of the XRB, we can now have the entire picture for the evolution of AGNs contributing to the XRB radiation. The most fundamental observational quantity describing the AGN evolution is a "luminosity function", the co-moving space density given as a function of luminosity and redshift. In order to determine an X-ray AGN luminosity function, straightforward but very time consuming work is required: we need to resolve the XRB into discrete AGNs, define statistical samples, and measure the redshift of each object as complete as possible, usually by means of optical spectroscopic observations.

The "hard" shape of the XRB spectrum, whose energy

density peaks around 30 keV, indicates that the majority of AGNs should be absorbed in X-rays. Hard X-ray surveys provide one of the most efficient and complete methods to pick up major AGN populations, since hard X-rays are much less affected by absorption or by dilution from star light in the host galaxy compared with soft X-rays or visible lights. X-ray absorbed AGNs are in most cases optical type-2 AGNs (i.e., those not showing broad emission lines) as expected from the unified scheme (Awaki et al., 1991), although the classification does not always match between in the X-ray and optical bands (e.g., Maiolino et al. 2001). Table 1 lists surveys conducted in hard X-ray band ($\gtrsim 3$ keV) with optical identification program in bright to medium flux range ($10^{-11} - 10^{-15}$ erg cm^{-2} s^{-1}in the 2–10 keV band). For comparison, the detection limit of each survey band is converted into the 2–10 keV flux by assuming a typical AGN spectrum of detected sources. (The list of "deep" surveys with Chandra and XMM is given in Table 1 of Brandt & Hasinger 2005.) Hard X-ray surveys can trace the evolution of both type-1 and type-2 AGNs and their number ratio as a function of luminosity and redshift. On the other hand, soft X-ray surveys generally reach fainter flux limits, although they are subject to biases against type-2 AGNs. Thus, hard-band and soft-band surveys are quite complementary each other. The latest result on soft X-ray luminosity function (SXLF) of type-1 AGNs is presented in Hasinger et al. (2005).

2. HARD X-RAY LUMINOSITY FUNCTION

To determine an X-ray AGN luminosity function in the wide luminosity and redshift range, it is important to use a combination of multiple surveys with different flux limits and survey area, in order to decouple luminosity and redshift dependences. Another key point is identification completeness of the sample used in the analysis. Figure 2 shows the correlation between hard X-ray and R-band fluxes for hard X-ray selected AGNs. As noticed, a significant fraction of X-ray sources with fluxes of $\sim 10^{-13}$ erg cm^{-2} s^{-1} (2–10 keV) have optical magnitudes of $R > 24$, for which spectroscopic identification is difficult even with 8-m class telescopes. This fact makes accurate determination of hard X-ray luminosity function (HXLF) more challenging than in soft X-rays. Several methods are adopted by different groups to correct for incompleteness in the calculation of HXLF:

1. Use only samples with high ($> 90\%$) completeness (Ueda et al. 2003, hereafter U03; Hasinger et al. 2005).
2. Obtain absolute upper limits on the AGN number density by putting all the unidentified sources at each redshift, although the limit may become not very constraining if the completeness is relatively low (see e.g., Cowie et al. 2003).
3. Consider optical and X-ray flux limit in the volume calculation (Hasinger et al., 2005).

Table 1. List of Hard X-ray Surveys in Bright to Medium Flux Range

Survey	Flux limit erg cm^{-2} s^{-1} (2-10 keV)	ref.
HEAO1 A2	3×10^{-11}	1
HEAO1 A1	2×10^{-11}	2
RXTE ASM	1×10^{-11}	3
Integral	$\approx 10^{-11}$	4
Swift BAT	$\approx 10^{-11} - 10^{-12}$	5
XMM Slew	4×10^{-12}	6
ASCA MSS	3×10^{-13}	7
ASCA LSS	1×10^{-13}	8
BeppoSAX HELLAS	1×10^{-13}	9
XMM Bright	9×10^{-14}	10
ASCA Deep	4×10^{-14}	11
XMM Medium	2×10^{-14}	12
XMM LSS	2×10^{-14}	13
Chandra LSS	$\approx 10^{-14}$	14
HELASS2XMM	8×10^{-15}	15
CLASXS	4×10^{-15}	16
ChaMP	3×10^{-15}	17
CYDER	2×10^{-15}	18
SEXSI	$\approx 10^{-15}$	19
Chandra/XMM Deep	$10^{-15} - 2 \times 10^{-16}$	20

References: 1. Piccinotti et al. (1982) 2. Grossan (1992) 3. Revnivtsev et al. (2004) 4. Beckmann et al. (2005) 5. Markwardt et al. (2005) 6. Saxton et al. (2005) 7. Ueda et al. (2001; 2005) 8. Ueda et al. (1999) 9. Fiore et al. (1999) 10. Della Ceca et al. (2004) 11. Ishisaki et al. (2001), Ohta et al. (2003) 12. Barcons et al. (2002) 13. Chiappetti et al. (2005) 14. Murray et al. (2004) 15. Fiore et al. (2003) 16. Steffen et al. (2004) 17. Kim et al. (2004) 18. Treister et al. (2005) 19. Harrison et al. (2003) 20. Brandt & Hasinger (2005) and references therein

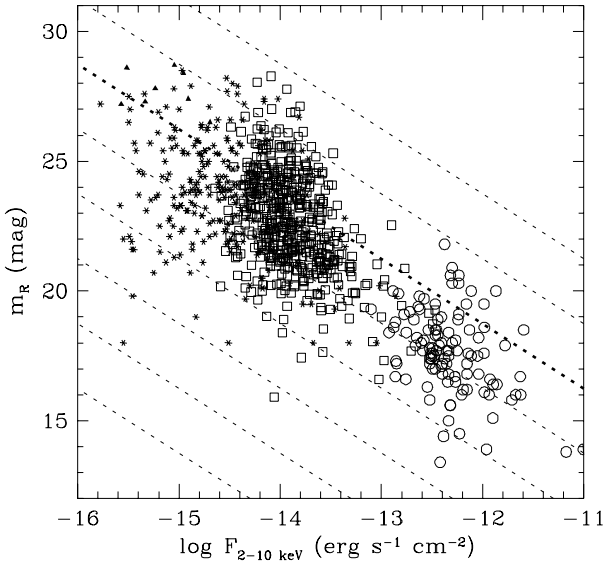

Figure 2. The 2–10 keV flux versus R-band magnitude diagram for hard X-ray selected samples. Asterisk: from Chandra deep field north (Barger et al., 2003) and Chandra deep field south (Szokoly et al., 2004). Squares: from the Subaru-XMM deep survey (Akiyama et al., in prep). Circles: from ASCA surveys (Akiyama et al. 2000; Akiyama et al. 2003).

4. Make area correction in the X-ray flux versus optical flux plane. In this method there is an implicit assumption that the unidentified sources have the same redshift distribution of that of identified sources. Adopted by Silverman et al. (2005).
5. Consider the correlation between X-ray luminosity and optical luminosity. There is an implicit assumption that the same correlation found from low redshift objects holds at higher redshift. Adopted by La Franca et al. (2005).

Studies using hard X-ray selected AGNs reveal that the comoving space density of AGNs (type-1 and type-2) shows evolution that differs with luminosity range (e.g., Cowie et al. 2003, Fiore et al. 2003, U03, Steffen et al. 2003). With a highly complete hard X-ray selected sample consisting of 243 AGNs detected with HEAO-1, ASCA, and Chandra, U03 have found that the overall AGN evolution in the luminosity range of Log $L_{\rm X}$ = $41.5 - 46.5$ over z=0–3 can be well described by the luminosity dependent density evolution (LDDE), where the cutoff redshift above which the density evolution terminates increases with luminosity. Representing the present-day HXLF with smoothly-connected two power-law form,

$$\frac{{\rm d}\Phi(L_{\rm X}, z=0)}{{\rm dLog}L_{\rm X}} = A[(L_{\rm X}/L_*)^{\gamma 1} + (L_{\rm X}/L_*)^{\gamma 2}]^{-1}, \quad (1)$$

they model the evolution as

$$\frac{{\rm d}\Phi(L_{\rm X}, z)}{{\rm dLog}L_{\rm X}} = \frac{{\rm d}\Phi(L_{\rm X}, 0)}{{\rm dLog}L_{\rm X}} e(z, L_{\rm X}), \quad (2)$$

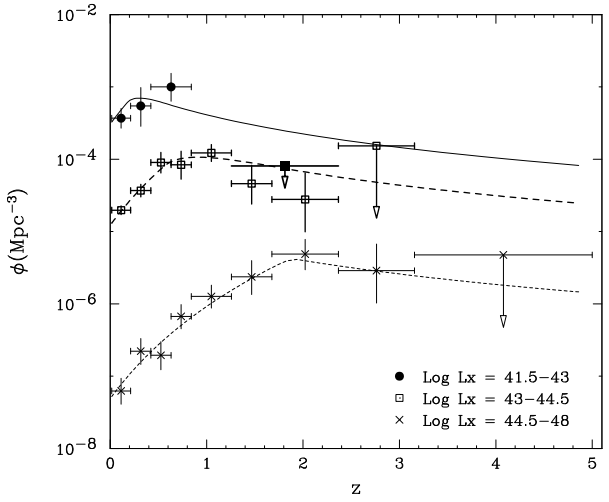

Figure 3. The comoving spatial density of AGNs as a function of redshift in three luminosity ranges, Log $L_{\rm X}$ =41.5–43 (upper), 43–44.5 (middle), 44.5–48 (lower), taken after U03. The lines are calculated from their best-fit HXLF. The errors are 1σ, while the long arrows denote the 90% upper limits (corresponding to 2.3 objects). The short arrow (marked with a filled square, red) corresponds to the 90% upper limit on the average spatial density of AGNs with Log $L_{\rm X}$ =43–44.5 at z=1.2–2.3 when all the unidentified sources are assumed to be in this redshift bin.

where

$$e(z, L_{\rm X}) = \begin{cases} (1+z)^{p1} & (z \le z_{\rm c}(L_{\rm X})) \\ e(z_{\rm c})(\frac{1+z}{1+z_{\rm c}(L_{\rm X})})^{p2} & (z > z_{\rm c}(L_{\rm X})) \end{cases}$$

and the cut-off redshift can be approximated as

$$z_{\rm c}(L_{\rm X}) = \begin{cases} z_{\rm c}^* & (L_{\rm X} \ge L_a) \\ z_{\rm c}^*(L_{\rm X}/L_a)^{\alpha} & (L_{\rm X} < L_a). \end{cases}$$

The best-fit parameters obtained by U03 are $A = 5.04 \pm 0.33$ [10^{-6} h_{70}^3 Mpc^{-3}], Log L_* = $43.94^{+0.21}_{-0.26}$, γ_1 = 0.86±0.15, γ_2 = 2.23±0.13, $p1$ = 4.23±0.39, α= 0.335±0.070 for fixed values of $p2 = -1.5$, $z_{\rm c}^* = 1.9$, and Log $L_a = 44.6$. Figure 3 shows the comoving spatial density of all Compton-thin AGNs as a function of redshift in different luminosity ranges. This behavior is essentially confirmed by La Franca et al. (2005) who added the CDFS and HELLAS2XMM samples in the similar analysis. The LDDE also gives a good representation of the SXLF of type-1 AGNs (Hasinger et al., 2005), as shown earlier by Miyaji et al. (2000) but with slightly different parameterization. Barger et al. (2005) argue that the HXLF at $z < 1.2$ is consistent with pure luminosity evolution (PLE), which is often used to model optical luminosity functions of type-1 quasars (e.g., Croom et al. 2004). The PLE does not, however, describe the overall evolution of XLF in the wider redshift range from $z = 0$ to z=3–5 (e.g., U03; Hasinger et al. 2005).

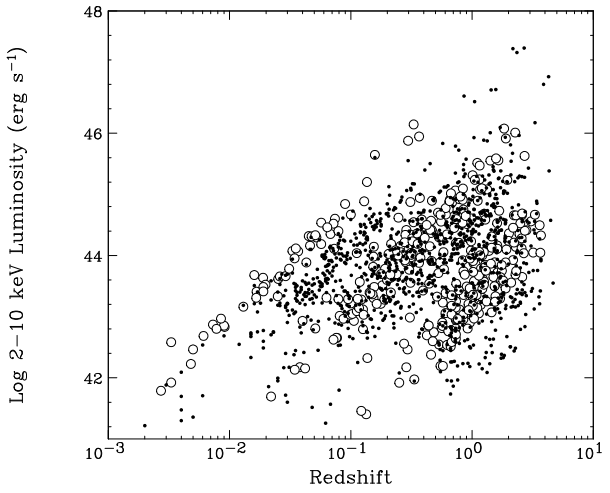

Figure 4. The redshift versus luminosity plot for the soft+hard combined sample. The luminosity $L_{\rm X}$ is an "intrinsic" one in the rest frame 2–10 keV band before being absorbed. Filled circles: soft-band selected AGNs. Open circles: hard-band selected AGNs.

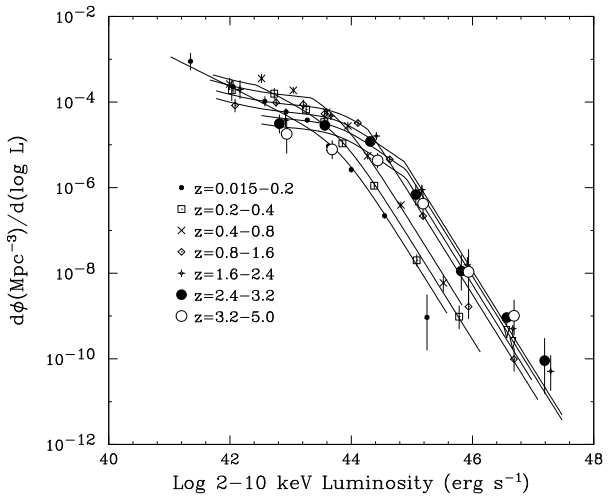

Figure 5. The intrinsic 2–10 keV luminosity function of all the Compton-thin AGNs determined from the combined analysis of the hard and soft X-ray selected samples. The curves represent the best-fit LDDE model. The data are plotted with 1σ Poisson errors.

To determine the AGN XLF in the rest frame 2–10 keV band with the best accuracy, a combined analysis using both hard-band and soft-band selected AGNs is now ongoing (Ueda et al. in prep.). The combined sample consists of 1341 sources in total selected from extended samples used in U03 and Hasinger et al. (2005). We utilize a maximum likelihood method to reproduce the count-rate versus redshift distribution for each survey, taking account of all selection effects. Figure 4 shows the redshift-luminosity diagram of the combined sample. The best-fit XLF is plotted in Figure 5 for different redshift ranges.

The LDDE of AGNs, where the peak redshift increases with luminosity, indicates that SMBHs finally growing to larger mass formed earlier than smaller mass ones. This fact is apparently contradictory to a naive expectation from the standard, hierarchical structure-formation theory of the universe where larger mass dark halo formed later as the consequence of bottom-up growth. Thus, the AGN evolution is called "anti-hierarchical" growth or "down-sizing". Note that evidence for down-sizing is also seen in the star-formation history (e.g., Cowie et al. 1996, Heavens et al. 2004, Kodama et al. 2004). These results challenge theories of SMBH and galaxy formation, requiring consideration of physical processes of baryons, such as feedback of AGNs and/or supernova to the accretion and star formation. Several theoretical models or simulations that reproduce the anti-hierarchical evolution have been proposed (e.g., Di Matteo et al. 2003, Granato et al. 2004, Hopkins et al. 2005).

3. LUMINOSITY DEPENDENCE OF THE ABSORBED-AGN FRACTION

The ratio of absorbed to unabsorbed AGNs (or optical type-1 to type-2 AGNs) is another key issue for AGN evolution, which is described by the column-density distribution function ($N_{\rm H}$ function; see U03). U03 find from their hard X-ray selected sample that the fraction of absorbed AGNs (Log $N_{\rm H}$<22) in the total (Compton-thin) AGNs decreases with luminosity. The trend was pointed out by Lawrence & Elvis (1982), and is consistent with the deficiency of luminous, absorbed AGNs in the ASCA and HEAO1 surveys (e.g., Akiyama et al. 2000; Shinozaki et al. 2005). Similarly, the fraction of optical type-1 AGNs in total AGNs also decreases at low luminosity (Steffen et al. 2003; Barger et al. 2005). The result indicates that simple extension of the "unified scheme" to higher luminosity where the fraction of absorbed AGNs is assumed to be constant needs to be modified, and is consistent with population synthesis of the XRB (U03; Treister & Urry 2005). In addition to the luminosity dependence, La Franca et al. (2005) recently claim that the absorbed-AGN fraction increases toward higher redshift.

4. THE ACCRETION HISTORY OF THE UNIVERSE

The HXLF of type-1 and type-2 AGNs provides strong observational constraints on the growth history of SMBHs through accretion. The bolometric luminosity $L_{\rm bol}$ of an AGN is related to the mass accretion rate through the mass-to-energy conversion factor ϵ as

$$L_{\rm bol}(\equiv \eta L_{\rm Edd}) = \epsilon \dot{M} c^2. \quad (3)$$

Here η is the Eddington ratio. As argued by Soltan (1982), the evolution of total accreted mass density, $\rho(z)$, is related to the HXLF as

$$\rho(z) = \int_{z_{\rm max}}^{z} \frac{(1-\epsilon)\dot{\lambda}(z)}{\epsilon c^2}(\frac{dt}{dz})dz, \qquad (4)$$

where

$$\dot{\lambda}(z) = \int L_{\rm bol}\Phi(L_{\rm X}, z)d{\rm Log}L_{\rm X} \qquad (5)$$

is the comoving bolometric luminosity density. Thus, comparison of $\rho(0)$ with the local black hole mass density independently estimated from the $M-\sigma$ relation can be used to constrain ϵ. It is essential to use a luminosity function of all AGNs including type-2 objects, otherwise $\rho(z)$ would be significantly underestimated. Previous studies (Salluci et al. 1999; Elvis et al. 2002), estimated $\rho(0)$ from the hard XRB intensity assuming a single effective redshift for the XRB sources. Now the HXLF has been observationally determined, which enables us to obtain $\rho(z)$ more accurately by integrating the formula (4).

To calculate $\dot{\lambda}$, an X-ray luminosity must be converted to a bolometric one, $L_{\rm bol}$. This correction is an issue, however, because the spectral energy distribution (SED) of AGNs has large scatter, depends on luminosity, and could be affected by selection biases in the survey band (see the discussion in Hasinger 2005). Phenomenological models for AGN SED are proposed by e.g., Marconi et al. (2004) and Shankar et al. (2004). Here, assuming the relation $L_{\rm X} \propto L_{\rm B}^{0.9}$ between the 2–10 keV and B-band luminosity obtained from a large X-ray selected sample (Anderson et al., 2003), we consider two extreme cases: the bolometric luminosity is proportional to the B-band luminosity, $L_{\rm bol} = 11.8\nu_{\rm B}L_{\rm B}[= 4.5\times10^{45}(\frac{L_{\rm X}}{10^{44}})^{1/0.9}]$ (case I), where $\nu_{\rm B}$ is the B-band frequency, and to the 2–10 keV luminosity, $L_{\rm bol} = 30L_{\rm X}$ (case II). The correction factors are based on the averaged spectrum of quasars complied by Elvis et al. (1994). The difference between the two cases would give an estimate for the uncertainty in the bolometric correction.

Figure 6 shows the results of $\dot{\lambda}$(z) and $\rho(z)$ obtained from the U03 HXLF (thick lines for case I and thin lines for case II) by assuming $\epsilon = 0.1$ and $z_{\rm max} = 5$. The dashed lines correspond to the case when 1.6 times as many Compton-thick AGNs as those with Log $N_{\rm H}$ = 23–24 are included according to the result by Risaliti et al. (1999). Compared with the results of $\rho(z)$ by Yu & Tremaine (2002), where the optical luminosity function of type-1 quasars by Boyle et al. (2000) is utilized, the mass growth continues more significantly after $z < 1$, owning to the contribution from absorbed, low luminosity AGNs. The estimated total accreted mass density is $\rho(0)$ = $(2.2-5.3)\times10^5$ $\rm M_\odot Mpc^{-3}$, in agreement with that of the local black hole mass density of $(4.2\pm1.1)\times10^5$ $\rm M_\odot Mpc^{-3}$ (Shankar et al., 2004). Further, Marconi et al. (2004) compared the accreted black hole mass function (BHMF) derived from the continuity equation with the local BHMF, and obtained that $\epsilon \approx 0.1$ and $\eta \approx 1$ (see also Shankar et al. 2004 who introduce the redshift

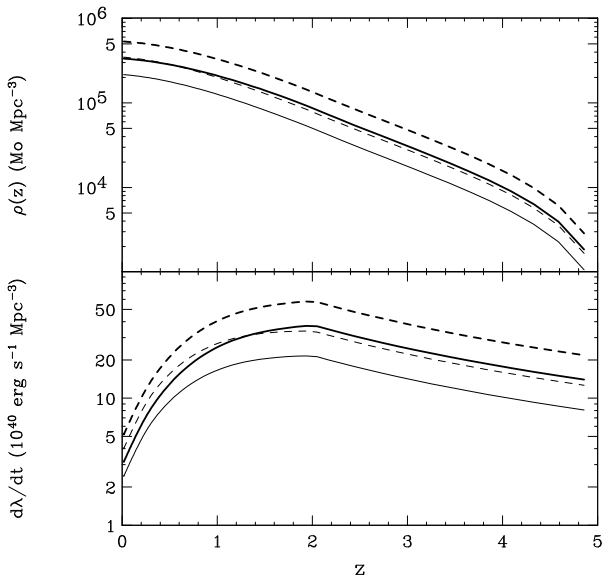

Figure 6. Upper panel: the growth curve of SMBHs traced by the U03 HXLF (total accreted mass density as a function of redshift). The mass-to-energy conversion factor $\epsilon = 0.1$ is assumed. Lower panel: evolution of the comoving bolometric luminosity density for $L_{\rm X} > 10^{41.5}$ erg s^{-1}. The HXLF model is extrapolated to the range of $z > 3$. Solid line: only Compton-thin AGNs are considered. Dashed line: Compton-thick AGNs are included. The bolometric correction is made assuming $L_{\rm bol} = 11.8L_{\rm B} \propto L_{\rm X}^{1/0.9}$ (case I: thick lines) and $L_{\rm bol} = 30L_{\rm X}$ (case II: thin lines).

dependence for η). Tamura et al. (2005) show that the accreted BHMF at $z \simeq 1$ with $\epsilon = 0.1$ and $\eta = 1$ is broadly consistent with the BHMF estimated from early-type galaxy luminosity functions at the redshift. These results suggest that the standard accretion with $\epsilon \simeq 0.1$ is the major process for the overall growth of SMBHs. However, considering the uncertainties particularly in the bolometric correction and Compton-thick AGN fraction, partial contribution from other accretion mode (such as radiatively inefficient accretion flow) is not entirely excluded, which could be important in the early stage of BH growth (e.g.,Kawaguchi et al. 2004).

5. SUMMARY

Thanks to the continuous efforts for 43 years since the beginning of X-ray astronomy, we might be able to say that the origin of the XRB is almost solved at energies below $\simeq$6 keV. Population synthesis models that takes into the HXLF and $N_{\rm H}$ function are now close to finalization with fine parameter tuning (see also Gilli 2005, this volume). However, when referring to "models", one always has to keep in mind which are direct observational facts and which are assumptions. In fact, a significant portion of the XRB above 6 keV has not been resolved into discrete sources even in the currently deepest sur-

veys (Worsley et al., 2005), for which discussion still relies on extrapolation from observational results at lower energies. For instance, the shape of the $N_{\rm H}$ function including Compton-thick regimes (Log $N_{\rm H}$ >24) has large uncertainties even in the local universe, and its evolution must be examined by much larger hard X-ray selected samples. The fraction of Compton-thick AGNs has direct impact on the accretion history of the universe. In population synthesis models that reproduce shape of the XRB spectrum, the assumed number of Compton-thick AGNs strongly couples with the mean amount of the reflection component, for which our knowledge is still limited. Obviously, higher sensitivity observations at energies above $\simeq 10$ keV are indispensable to address the remaining issues of the XRB.

ACKNOWLEDGEMENTS

I would like to thank my colleagues in this field for stimulating discussion. I am grateful to my collaborators for their help for this presentation, especially Masayuki Akiyama, Kouji Ohta, Takamitsu Miyaji, Yoshitaka Ishisaki, and Günther Hasinger.

REFERENCES

Akiyama, M., et al. 2000, ApJ, 532, 700

Akiyama, M., et al. 2003, ApJS, 148, 275

Anderson, S. F. et al. 2003, AJ, 126, 2209.

Awaki, H., Koyama, K., Inoue, H., & Halpern, J.P. 1991, PASJ, 43, 195

Barcons, X., et al. 2002, A&A, 382, 522

Barger, A.J., et al. 2003, AJ, 126, 632

Barger, A.J., et al. 2005, AJ, 129, 578

Beckmann, V, Gehrels, N., Shrader, C.R., Soldi, S. ApJ, 2005, in press

Boyle, B.J., et al. 2000, MNRAS, 317, 1014, 2000

Brandt, W.N., & Hasinger, G. 2005, ARA&A, 43, 827

Chiappetti, L. et al. 2005, A&A, 439, 413

Cowie, L.L., Songaila, A., Hu, E.M., Cohen, J.G. 1996, AJ, 112, 839

Cowie, L.L., et al. 2003, ApJ, 584, L57

Croom, S.M., et al. 2004, MNRAS, 349, 1397

Della Ceca, R., et al. 2004, A&A, 428, 383

Di Matteo, T., Croft, R.A.C., Springel, V., Hernquist, L. 2003, ApJ, 593, 56

Elvis, M., et al. 1994, ApJS, 95, 1.

Elvis, M., Risaliti, G., & Zamorani, G. 2002, ApJ, 565, L75.

Fabian, A.C., & Iwasawa, K., 1999, MNRAS, 303, L34

Fiore, F., et al. 1999, MNRAS, 306, L55

Fiore, F., et al. 2003, A&A, 409, 79

Granato, G.L., et al. 2004, ApJ, 600, 580

Grossan, B., 1992, PhD thesis, MIT

Harrison, F. A., Eckart, M. E., Mao, P. H., Helfand, D. J., & Stern, D. 2003, ApJ, 596, 944

Hasinger, G., 2005, in "Growing black holes", Merloni, A., Nayakshin S., Sunyaev R.A. (Eds.). Berlin: Springer, p. 418 (astro-ph/0412576)

Hasinger, G., Miyaji, T., Schmidt, M. 2005, A&A, 441, 417

Heavens, A., Panter, B., Jimenez, R., Dunlop, J. 2004, Nature, 428, 625

Hopkins, P.F., et al. 2005, ApJ, in press (astro-ph/0506398)

Ishisaki, Y., et al. 2001, PASJ, 53, 445

Kawaguchi, T. et al. 2004, A&A, 420, L23

Kim, D.-W., et al. 2004, ApJS, 150, 19

Kodama, T. et al. 2004, MNRAS, 350, 1005

Kushino, A., et al. 2002, PASJ, 54, 327

La Franca, F., et al. 2005, ApJ, in press

Lawrence, A. & Elvis, M. 1982, ApJ, 256, 410

Maiolino, R., et al. 2001, A&A, 365, 28

Marconi, A. et al. 2004, MNRAS, 351, 169

Markwardt, C.B., et al. 2005, ApJL, in press

Miyaji, T., Hasinger, G., & Schmidt, M. 2000, A&A, 353, 25

Murray, S.S. et al. 2004, SPIE, 5488, 242

Ohta, K., et al. 2003, ApJ, 598, 210

Piccinotti, G., et al. 1982, ApJ, 253, 485

Revnivtsev, M., Sazonov, S., Jahoda, K., & Gilfanov, M. 2004, A&A, 418, 927

Risaliti, G., Maiolino, R., & Salvati, M. 1999, ApJ, 522, 157

Salluci, P., Szuszkiewicz, E, Monaco, P., & Danese, L. 1999, MNRAS, 307 637

Saxton, R.D., et al. 2005, SPIE 5898, 73

Shankar, F., et al. 2004, MNRAS, 354, 1020

Shinozaki, K., et al. 2005, AJ, submitted

Silverman, J.D. et al. 2005, ApJ, 624, 630

Soltan, A. 1982, MNRAS, 200, 115

Steffen, A.T., et al. 2003, ApJ, 596, L23

Steffen, A.T., et al. 2004, AJ, 128, 1483

Szokoly, G.P., et al. 2004, ApJS, 155, 271

Tamura, N., Ohta, K., Ueda, Y. 2005, MNRAS, in press

Treister, E., et al. 2005, ApJ, 621, 104

Treister, E., & Urry, C.M. 2005, ApJ, 630, 115

Ueda, Y., et al. 1999, ApJ, 518, 656

Ueda, Y., Ishisaki, Y., Takahashi, T., Makishima, K., & Ohashi, T. 2001, ApJS, 133, 1

Ueda, Y., Akiyama, M., Ohta, K., & Miyaji, T. 2003, ApJ, 598, 886 (U03)

Ueda, Y., Ishisaki, Y., Takahashi, T., Makishima, K., & Ohashi, T. 2005, ApJS, in press

Worsley, M.A. et al. 2005, MNRAS, 357, 1281

Yu, Q. & Tremaine, S. 2002, MNRAS, 335, 965